nature communications

Article

https://doi.org/10.1038/s41467-025-60543-5

Memantine inhibits calcium-permeable AMPA receptors

Received: 13 October 2024

Accepted: 26 May 2025

Published online: 01 July 2025

Check for updates

Elisa Carrillo[1] ✉, Alejandra Montaño Romero[2,3], Cuauhtemoc U. Gonzalez[1,4], Andreea L. Turcu[5], Santiago Vázquez[5], Edward C. Twomey[2,3,6,7] ✉ & Vasanthi Jayaraman[1,4] ✉

Memantine is an US Food and Drug Administration (FDA) approved drug that is thought to selectively inhibit NMDA-subtype of ionotropic glutamate receptors (NMDARs). NMDARs enable calcium influx into neurons and are critical for normal brain function. However, increasing evidence shows that calcium influx in neurological diseases is augmented by calcium-permeable AMPA-subtype ionotropic glutamate receptors (AMPARs). Here, we demonstrate that these calcium-permeable AMPARs (CP-AMPARs) are inhibited by memantine. Electrophysiology unveils that memantine inhibition of CP-AMPARs is dependent on their calcium permeability and the presence of their neuronal auxiliary subunit transmembrane AMPAR regulatory proteins (TARPs). Through cryo-electron microscopy we elucidate that memantine blocks CP-AMPAR ion channels in a unique mechanism of action from NMDARs. Furthermore, we demonstrate that memantine inhibits a gain of function AMPAR mutation found in a patient with a neurodevelopmental disorder. Our findings unlock potential exploitation of this site to design more specific drugs targeting CP-AMPARs.

Ionotropic glutamate receptors are the primary mediators of excitatory transmission in the mammalian central nervous system[1,2]. They are broadly classified into four subtypes: amino-3-hydroxy-5-methyl-4-isoxazolepropionic acid (AMPA), N-methyl-D-aspartate (NMDA), kainate, and delta receptors[1,3]. AMPA receptors (AMPARs) mediate fast synaptic signaling and are predominantly calcium impermeable[1,2]. AMPARs are formed by combinations of four subunits: GluA1, GluA2, GluA3, and GluA4, which can assemble as homomeric or heteromeric combinations[1]. GluA2 is unique among these subunits as it exists predominantly in an edited form where the glutamine residue at site 607 (referred to as the Q/R site) is edited to arginine[4]. The Q/R edited version of GluA2 confers calcium impermeability in AMPARs. Most AMPARs in the mammalian central nervous system contain this edited GluA2 subunit, making them mostly calcium impermeable[1].

However, in various neuropathological conditions, there is an increase in the fraction of calcium-permeable AMPARs (CP-AMPARs)[5]. Specifically, down-regulation in RNA editing at the Q/R site of GluA2 has been associated with Alzheimer's disease[6], sporadic and familial amyotrophic lateral sclerosis[7], seizure vulnerability[8], and in malignant gliomas[9]. Additionally, a decrease in overall GluA2 subunits and an increase in the proportion of CP-AMPARs formed from a combination of GluA1, GluA3, and GluA4 receptors have been shown in pathological conditions such as neuropathic pain[10], and in ALS[11]. The changes in GluA2 editing and/or protein levels lead to an increase of CP-AMPARs

[1]Center for Membrane Biology, Department of Biochemistry and Molecular Biology, University of Texas Health Science Center at Houston, Houston, TX, USA. [2]Department of Biophysics and Biophysical Chemistry, Johns Hopkins University School of Medicine, Baltimore, MD, USA. [3]Solomon H. Snyder Department of Neuroscience, Johns Hopkins University School of Medicine, Baltimore, MD, USA. [4]MD Anderson Cancer Center UTHealth Graduate School of Biomedical Sciences, University of Texas Health Science Center at Houston, Houston, TX, USA. [5]Laboratori de Química Farmacèutica (Unitat Associada al CSIC), Facultat de Farmàcia i Ciències de l'Alimentació i Institut de Biomedicina (IBUB), Universitat de Barcelona, Av. Joan XXIII, 27-31, 08028 Barcelona, Spain. [6]The Beckman Center for Cryo-EM at Johns Hopkins, Johns Hopkins University School of Medicine, Baltimore, MD, USA. [7]Diana Helis Henry Medical Research Foundation, New Orleans, LA, USA. ✉e-mail: elisa.carrilloflores@uth.tmc.edu; twomey@jhmi.edu; vasanthi.jayaraman@uth.tmc.edu

https://doi.org/10.1038/s41467-025-60543-5

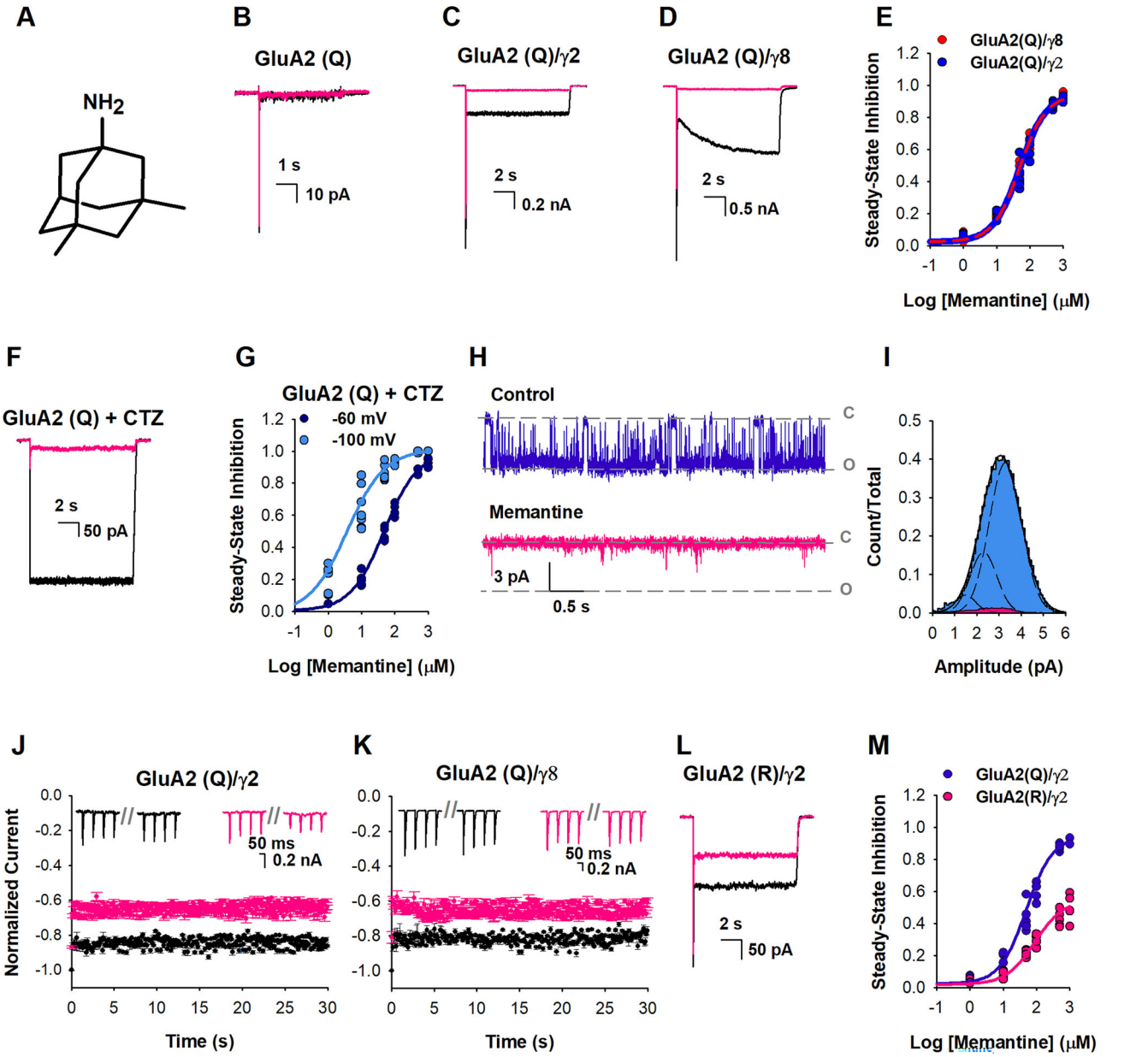

Fig. 1 | Memantine inhibition of AMPA receptors. A Chemical structure of memantine. Representative current traces due to 10 mM glutamate in the absence (black) and presence of 500 μM memantine (pink) from HEK-293 cells expressing (**B**) GluA2(Q), (**C**) GluA2(Q)/γ2, (**D**) GluA2(Q)/γ8. **E** The dose-dependent inhibitory effects of memantine on GluA2 (Q)/γ2 with IC_{50} 49 ± 2 μM (blue), and GluA2 (Q)/γ8 with IC_{50} 48 ± 3 μM (pink). Each dot represents data from a different cell. **F** Representative current trace for GluA2(Q) due to 10 mM glutamate in the presence of 100 μM CTZ and in the absence (black) and presence of 500 μM memantine (pink). **G** The dose-dependent memantine inhibition on GluA2(Q) in the presence of CTZ at −60 (dark blue) and −100 mV (light blue), with IC_{50} 48 ± 3 μM and 4.1 ± 1.3 μM, respectively. Each dot represents data from a different cell. **H** Single-channel currents were recorded from GluA2(Q) in the presence of 100 μM CTZ during continuous application of 10 mM glutamate alone (blue) and in the presence 500 μM of memantine (pink) at −100 mV. Openings are shown as downward deflections. **I** Amplitude histogram from the single channel recordings ($n = 5$). Effect of memantine under 10 Hz frequency stimulation with 10 mM glutamate alone (black) or in the presence of 10 μM of memantine (pink) for (**J**) GluA2(Q)/γ2 ($n = 4$) and (**K**) GluA2(Q)/γ8 ($n = 4$); $p = 0.00023$ and 0.00036 respectively. Data are shown as mean ± SEM. **L** Representative current trace for GluA2(R)/γ2 due to 10 mM glutamate in the absence (black) and presence of 500 μM memantine (pink). **M** The dose-dependent inhibitory effects of memantine on GluA2 (R)/γ2 with IC_{50} 1129 ± 85 μM (blue), compared to GluA2 (Q)/γ2 with IC_{50} 49 ± 2 μM (pink). Each dot represents data from a different cell.

in these neurological disorders, highlighting the need for pharmacological agents that can inhibit their activity.

Memantine (Fig. 1A) has been previously thought to be a selective inhibitor of NMDA receptors (NMDARs), with no significant effect on AMPARs[12,13]. Memantine inhibits NMDARs by acting as a blocker of the NMDAR ion channel[12,13]. Memantine also blocks acetylcholine receptor[14] and serotonin signaling[15]. In addition, double mutants at L577W along with arginine or threonine at the Q site in GluA1 have also been shown to be inhibited by micromolar concentrations of memantine[16]. The lack of memantine inhibition for AMPARs in prior experiments in neurons may be because they express predominantly calcium-impermeable AMPARs (CI-AMPARs)[13]. Furthermore, the initial electrophysiology studies on AMPARs in over-expressed systems were performed in the absence of auxiliary subunits[16], while physiological AMPARs are associated with auxiliary subunits[17,18]. These auxiliary subunits alter the biophysical and structural properties of the receptors[2,18–24]. In particular, the highly

prevalent auxiliary subunits transmembrane AMPAR regulatory proteins (TARP)-γ2 and -γ8, stabilize the open state of the receptor[2,20,23]. Given the increased appreciation for CP-AMPARs in neurological diseases, we hypothesized that memantine may have polypharmacology and also act through inhibiting CP-AMPARs.

Here we show that memantine inhibits CP-AMPARs in micromolar concentrations through electrophysiology and cryo-electron microscopy (cryo-EM). While CP-AMPARs are inhibited at tens of micromolar concentration, CI-AMPARs are inhibited only at hundreds of micromolar concentrations of memantine even in the presence of auxiliary subunits γ2 and γ8. We also show that memantine more effectively inhibits CP-AMPARs containing patient mutation at the ion channel selectivity filter. This mutation causes significant neurodevelopmental disorders[25], and thus memantine has a potential utility in inhibiting gain-of-function mutations such as this. Cryo-EM of activated CP-AMPARs in the presence of memantine shows that memantine directly interacts with the AMPAR Q/R site while sitting in the hydrophobic pocket of the ion channel, and inhibits CP-AMPARs through rearrangement of the selectivity filter. This mechanism is unique from polyamine-based pore blockers of CP-AMPARs. The structure also provides insight into why memantine inhibits the gain of function patient mutation. Our findings provides structural insight into the mechanism of inhibition by memantine, thus laying new foundations for therapeutic design.

Results

Memantine inhibition of CP-AMPARs requires auxiliary subunits

We recorded whole-cell currents induced by 10 mM glutamate from HEK-293 cells expressing the CP-AMPARs, homomeric GluA2(Q) under various conditions in the presence and absence of memantine. When GluA2(Q) receptors were studied in isolation the whole-cell currents induced by 10 mM glutamate did not show any significant inhibition even with 500 μM memantine (Fig. 1B). However, when auxiliary subunits γ2 (Fig. 1C) and γ8 (Fig. 1D) were present, both the peak and steady-state currents of GluA2(Q) receptors were inhibited by 500 μM memantine. The IC_{50} value for memantine inhibition for GluA2(Q) in the presence of γ2 was similar to that in the presence of γ8, 49 ± 2 μM and 48 ± 3, respectively (Fig. 1E). These data suggest that memantine inhibition requires the presence of auxiliary subunits.

The presence of auxiliary subunits γ2 or γ8 stabilizes the AMPAR open state and reduces the rate and extent of desensitization seen in GluA2(Q) receptors. Thus the inhibition by memantine under these conditions suggests that memantine inhibits the open channel form of the receptor. To test this idea, we studied inhibition by memantine of GluA2(Q) in the open channel state using 100 μM cyclothiazide (CTZ), a positive allosteric modulator (Fig. 1F). Under these conditions, 500 μM memantine showed inhibition of the steady-state currents, consistent with the findings in experiments with γ2 and γ8, providing further confirmation that memantine can inhibit GluA2(Q) receptors when the open channel state of the receptor is stabilized. For GluA2(Q), the IC_{50} for memantine block in the presence of CTZ was 48 ± 3 μM (Fig. 1G). These values are similar to those observed in the presence of γ2 and γ8, thus supporting the open channel block mechanism. The extent of inhibition by memantine is also voltage-dependent with higher inhibition at more negative voltages (Fig. 1G). Dose-response curves show a decrease in IC_{50} at more negative voltages with IC_{50} being 4.1 ± 1.3 μM at −100 mV relative to 48 ± 3 μM at −60 mV for the GluA2(Q) (Fig. 1G). Given that the resting potential can vary from −60 mV to −85 mV depending on the neuronal subtype and even within parts of the neuron[26], micromolar concentrations of memantine is expected to have a significant inhibition at CP-AMPARs.

To characterize the inhibition mechanism at the single-channel level we performed outside-out single-channel recordings of GluA2(Q)/γ2. Single channels in the presence of CTZ and a saturating concentration of glutamate (10 mM) are predominantly open and populate the higher conductance levels (Fig. 1H, blue). In the presence of memantine, the openings were brief and populated lower conductance states (Fig. 1H, pink). Overall, the receptor does not populate high conductance states in the presence of memantine (Fig. 1I). These measurements further support the inhibition by binding to the open channel form of the receptor. We also studied memantine inhibition of GluA2(Q)/γ2 and GluA2(Q)/γ8 using 10 Hz train of brief, ~1 ms pulses to mimic synaptic transmission and show inhibition of the currents plateaus to a similar level as that seen in steady state currents for both inhibition by 10 μM (Fig. 1J, K).

We also investigated the inhibition by trimethylmemantine (TMM), a memantine derivative with three methyl groups at the amine and a permanent charge on the amine group. TMM (Fig. S1) shows a lower inhibition on GluA2(Q) receptors stabilized in the open state by CTZ (Fig. S1), relative to memantine under the same condition, with TMM having a higher IC_{50} value of 384 ± 8 μM. Additionally, TMM shows less inhibition at saturating concentrations relative to that observed with memantine (Fig. S1). These results suggest a possible role of steric hindrance due to the bulky trimethyl group at the amine site as the cause for reduction in the inhibition, further consistent with memantine being in the pore where it is expected to have steric constraints. This is also seen in the classical NMDA inhibition by N-alkyl derivatives of memantine compared to memantine[27].

Furthermore, we confirmed that memantine does not significantly inhibit CI-AMPARs. We studied memantine block with the representative CI-AMPAR GluA2(R) in the presence of γ2. These studies show that memantine has only a minor inhibitory effect at 500 μM concentrations (Fig. 1L). Dose-response curves for steady-state inhibition with varying memantine concentrations confirmed these results, indicating that the IC_{50} value for memantine inhibition was 20 times higher for the GluA2(R)/γ2 receptor compared to the GluA2(Q)/γ2 receptor (Fig. 1M). Even at saturating concentrations of memantine, GluA2(R)/γ2 receptors displayed only partial inhibition of the currents mediated by 10 mM glutamate (Fig. 1M).

Memantine also inhibited the GluA1 homomeric receptors, a subtype of AMPA receptors that are calcium permeable. The IC_{50} value for inhibition was 15 ± 2 μM and 10 ± 2 μM in the presence of γ2, and γ8, respectively (Fig. 2A–C), which is significantly lower ($p < 0.0001$ for both conditions) than that observed for GluA2(Q) homomeric receptors. While we cannot study the isolated GluA1/GluA2 heteromeric receptors, the predominant subtype of AMPA receptors in the mammalian central nervous system, we studied memantine inhibition using a co-expression of GluA1 and GluA2 receptors. Co-expression results in a combination of GluA1 homomeric, GluA2 homomeric and GluA1/GluA2 heteromeric receptors. The IC_{50} value for memantine inhibition in this mixed system in the presence of γ2, was 697 ± 149 μM for GluA1/GluA2(R) (Fig. 2E) and 23.5 ± 4.5 μM for GluA1/GluA2(Q) (Fig. S2). This indicates that GluA2 editing leads to a decrease in mematine inhibition even in the context of the heteromeric receptor.

Memantine inhibition at CP-AMPARs is unique from NMDARs

To determine if other NMDAR channel blockers inhibited CP-AMPARs, we tested the effect of MK801 and ketamine, both of which are high affinity (nanomolar) channel blocker of NMDARs. We show that even at hundreds of micromolar concentrations MK801 and ketamine have a minimal inhibitory effect on CP-AMPARs (Fig. S1). Thus, the observation of NMDAR blocker polypharmacology with CP-AMPARs may be unique to memantine.

Additionally, memantine has been shown to have two pathways and sites for inhibition in NMDARs, one pathway through an open channel block and a second pathway through the membrane[27]. The membrane inhibition pathway is mediated by the uncharged memantine which can be studied by increasing the pH. To investigate if a similar two pathway mechanism occurs in memantine inhibition in CP-AMPARs, we preincubated cells with memantine before activation with

https://doi.org/10.1038/s41467-025-60543-5

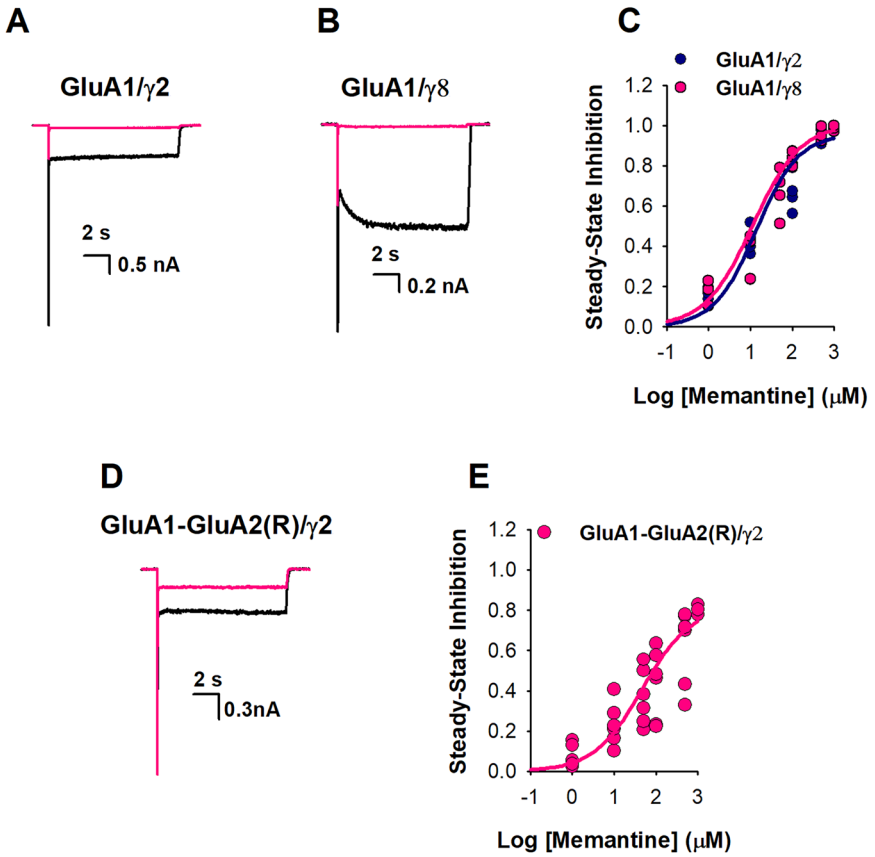

Fig. 2 | Memantine inhibition in the presence of GluA1 subtype. Representative current traces for GluA1/γ2 (**A**) and GluA1/γ8 (**B**) due to 10 mM glutamate in the absence (black) and presence of 500 μM memantine (pink). **C** The dose-dependent inhibitory effects of memantine on GluA1/γ2 with IC_{50} 15 ± 2 μM (blue), and GluA1/γ8 with IC_{50} 10 ± 2 μM (pink). **D** current traces for GluA1-GluA2(R)/γ2 due to 10 mM glutamate in the absence (black) and presence of 500 μM memantine (pink). **E** The dose-dependent inhibitory effects of memantine on GluA1-GluA2(R)/γ2 with IC_{50} 697 ± 149 μM (pink). Each dot represents data from a different cell.

10 mM glutamate in the presence of CTZ and compared the currents at pH 7.4 and pH 9. No significant differences were observed between pH 7.4 and pH 9 (Fig. S1). This suggests that, unlike what is observed in NMDARs, memantine does not block CP-AMPARs through a membrane pathway.

Mechanism of memantine channel block in CP-AMPARs

To elucidate the memantine channel block mechanism in CP-AMPARs, we used cryo-electron microscopy (cryo-EM) to capture activated CP-AMPARs in the presence of memantine. We used a well-established CP-AMPAR cryo-EM construct (GluA2-γ2$_{EM}$, Methods), which is a covalent fusion construct between GluA2(Q) and γ2. This construct has been extensively validated previously, both functionally and structurally, and has been utilized to study the structural basis of CP-AMPAR channel block[28–33].

We prepared samples for cryo-EM by activating GluA2-γ2$_{EM}$ in the presence of glutamate, CTZ, and memantine, which captured both the open channel memantine-blocked state (GluA2-γ2$_{mem}$) and open channel state without memantine (GluA2-γ2$_{open}$) (Fig. S3, Table S1). We found that 36,557 particles contribute to GluA2-γ2$_{mem}$ map, and 87,724 particles contribute to the GluA2-γ2$_{open}$ map. We hypothesize that less particles are memantine bound because cryo-EM specimen preparation is done without a membrane potential, and we observe that memantine block is voltage dependent.

GluA2-γ2$_{mem}$ and GluA2-γ2$_{open}$ are largely similar (root mean squared deviation, RMSD = 0.79 Å), with the exception of the transmembrane domain (TMD), where memantine binds. The overall architecture of GluA2-γ2$_{mem}$ is reminiscent of previously-solved GluA2-γ2 structures and native AMPAR complexes: at the core of GluA2-γ2$_{mem}$ are the CP-AMPAR GluA2(Q) subunits arranged in a tetramer, in complex with four γ2 subunits (Fig. 3A). There is an overall "Y" shape of the AMPAR, with the amino-terminal domain (ATD) and ligand binding domain (LBD) comprising the extracellular domain (ECD; Fig. 3A). The ECD in both GluA2-γ2$_{mem}$ and GluA2-γ2$_{open}$ is two-fold symmetric. Below the ECD is the TMD. In GluA2-γ2$_{open}$, the TMD is two-fold symmetric, as expected, similar to the originally solved open state of GluA2-γ2$_{EM}$[32]. The GluA2-γ2$_{mem}$ TMD is asymmetric due to a single copy of memantine in the AMPAR TMD (Fig. 3A).

The AMPAR ion channel is comprised of the M3 TMD helices and M2 helix, between which is the reentrant loop that contains the Q/R site and selectivity Filter (Fig. 3B). Memantine binds directly in the CP-AMPAR TMD immediately above the Q/R site, which is the primary determinant of ion channel selectivity in AMPARs. (Fig. 3B). The tricyclodecane backbone of memantine sits in the hydrophobic cavity of the ion channel, and the amine on memantine is directly coordinated by the glutamine residues at the Q/R site (Fig. 3B).

The cryo-EM map of GluA2-γ2$_{mem}$ directly shows the shape of memantine in the ion channel (Fig. 3B). This suggests a singular pose of memantine in the channel, similar to the structure of memantine bound to NMDARs. The memantine binding site is markedly absent from the GluA2-γ2$_{open}$ map (Fig. S4). The memantine binding site in GluA2-γ2$_{mem}$ is resolved to ~3–3.5 Å (Fig. S4). We suspect the difference in resolution between GluA2-γ2$_{open}$ and GluA2-γ2$_{mem}$ is due to the difference in particle numbers contributing to each respective reconstruction. Hydrophobic residues in each subunit coordinate the memantine tricyclodecane cage (Fig. 3C). Residues T617 in subunits A and B, as well as I613 in subunit C play the principal roles in coordination via the hydrophobic cavity and are within 4 Å of interaction with

https://doi.org/10.1038/s41467-025-60543-5

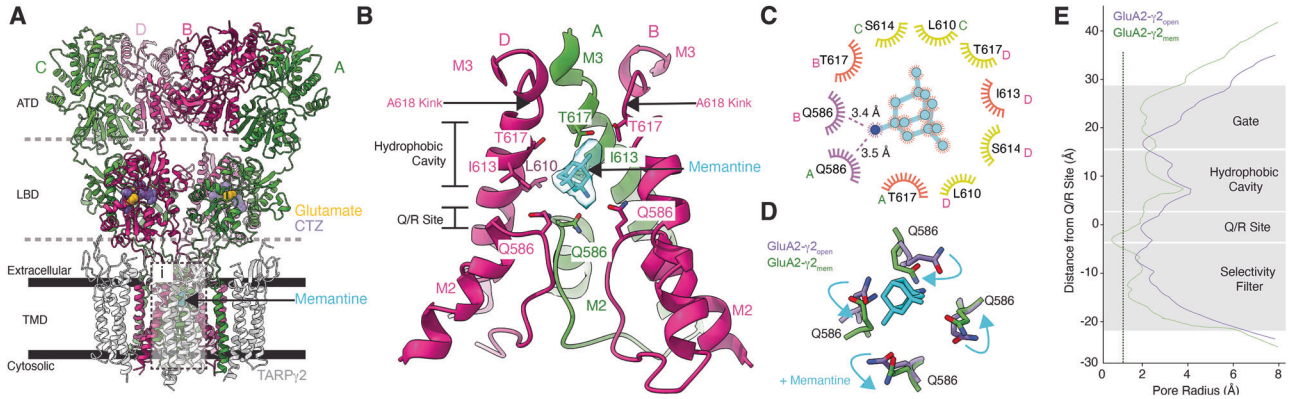

Fig. 3 | Memantine block revealed by Cryo-EM. A Overall architecture of GluA2-γ2$_{mem}$ in a ribbon diagram. GluA2 subunits are labeled depending on their positions (**A**, **C** are green; **B**, **D** are pink). γ2 subunits are colored white. Dashed lines indicate domain boundaries, solid bars indicate membrane boundaries. Glutamate (yellow), CTZ (purple), and memantine (cyan) are shown as space filling models. Inset i is where (**B**) highlights. **B** The GluA2-γ2$_{mem}$ ion channel with M2 and M3 helices. Subunit C is omitted for clarity. The cryo-EM map at the memantine binding site is shown transparently in cyan around the molecule. Critical binding residues are labeled. Carbon atoms are colored with the color of their respective subunit with oxygen in red, nitrogen in blue. **C** LigPlot of the memantine binding site. Potential polar contacts are indicated with purple eyelashes. Orange eyelashes indicate a distance within 4 Å from memantine. Yellow eyelashes indicate a distance from 4 to 6 Å. **D** How memantine rearranges the Q/R site; cyan arrows indicate changes from GluA2-γ2$_{open}$ (purple) to GluA2-γ2$_{mem}$ (green). **E** Pore radius plots of GluA2-γ2$_{open}$ (purple) and GluA2-γ2$_{mem}$ (green). Dashed line represents the radius of a calcium cation.

memantine. Interestingly, T617 residues are required for calcium coordination in the ion channel[34]. The presence of memantine at this position likely prevents that possibility. The amine group on memantine is directly coordinated by polar interactions with Q586, the Q607-equivalent in GluA2-γ2$_{EM}$, from subunits A and B. This is reflected in a rearrangement of the Q/R site in GluA2-γ2$_{mem}$ compared to GluA2-γ2$_{open}$ (Fig. 3D). Q586 from the A and B subunit positions move toward the pore center to coordinate memantine, while Q586 at the C and D positions move away from the pore. This overall rearrangement of the Q/R site constricts the remaining selectivity filter below the Q/R site compared to GluA2-γ2$_{open}$ (Fig. 3E).

The memantine binding site in GluA2-γ2$_{mem}$ directly shows why memantine has increased affinity for CP-AMPARs as opposed to CI-AMPARs. CI-AMPARs contain a bulky, positive charge via editing to ariginine at the Q/R site, which clashes directly with the charged amine group on memantine. And, glutamine at the Q/R site directly coordinates memantine in the pore.

The memantine block mechanism in CP-AMPARs is distinct from polyamine-based blockers. Polyamine blockers such as N, N, N-trimethyl-5-[(tricyclo[3.3.1.13,7]dec-1-ylmethyl)amino]−1-pentanaminium bromide hydrobromide (IEM-1460), 1-naphthyl acetyl spermine (NASPM), and Argiotoxin-636 (AgTx-636) block CP-AMPAR ion channels through permeating the selectivity filter with their polyamines, and plugging the channel via bulky hydrophobic headgroups that sit in the hydrophobic cavity (Fig. S5). Memantine blocks CP-AMPAR channels by sitting in the hydrophobic cavity, which ablates cation coordination in the upper vestibule of the channel, and by directly interacting with the Q/R site, which narrows the selectivity filter below.

Memantine binds to a similar site in NMDARs but is more closely coordinated by hydrophobic residues in the NMDAR ion channel[35]. This may account for the discrepancy in affinity between memantine inhibition in NMDARs versus CP-AMPARs. However, in contrast to inhibition in NMDARs, memantine rearranges the Q/R sites in CP-AMPARs, which occludes the channel.

Memantine inhibits a neurodevelopmental mutation in CP-AMPARs

In our cryo-EM data, we observe that memantine directly interacts with the GluA2 Q/R site. We hypothesized that by placing a negative charge at this site, we could dramatically increase the efficancy of memantine inhibition in AMPARs. In fact, there is a de novo mutation in a patient with severe developmental delays and Rett-like syndrome at the GluA2 Q/R site where glutamine is mutated to glutamate (GluA2(E); Q607E)[25]. The Q607E mutation causes a deleterious gain of function in AMPARs. Because memantine directly interacts with glutamine at the Q/R site, we hypothesized that memantine may have increased inhibition efficacy in GluA2(E). To test this idea, we investigated memantine inhibition of GluA2(E) AMPARs.

The extent of current inhibition for GluA2(E) in the presence of γ2 was notably higher than that observed for GluA2(Q) and GluA2(R) in the presence of γ2 (Fig. 4A). The IC_{50} for memantine inhibition was determined to be 25 ± 2 µM for GluA2(E) in the presence of γ2 (Fig. 4B), significantly lower than the values of 1129 ± 85 µM for the GluA2(R) in the presence of γ2 and 49.3 ± 2.4 µM for GluA2(Q) ($p < 0.0001$) in the presence of γ2 (Fig. 1E). The GluA2(E) also shows a voltage dependence with the IC_{50} for memantine GluA2(E) being shifted from 25 ± 2 µM to 5.7 ± 1 µM when the voltage was decreased from −60 mV to −100 mV (Fig. 4B). It is interesting to note that the voltage effect is not as significant in the GluA2(E) as in GluA(Q) mutant. It is possible that the larger effects due to the more negative membrane potential overrides the effect due to the charge change at GluA2(E). However, the exact mechanism will require further investigation.

We also studied memantine inhibition of another gain of function mutant "lurcher" GluA2 A622T and show that the IC_{50} (49 ± 5 µM) for the inhibition of this receptor which is not significantly different from that observed in the wild type GluA2(Q) subtype (Fig. S2) ($p = 0.7433$). This suggests that the higher inhibition observed for Q607E at −60 mV is specific to this mutation and not seen for the lurcher mutation.

The observed trends of greater inhibition current extent and a lower IC_{50} value for GluA2(E) compared to GluA2(Q)/γ2, and GluA2 lurcher, followed by GluA2(R), at −60 mV indicates that the charge at site 607 influences the extent of memantine inhibition, suggesting that positively charged amine group may reside close to 607 site. We performed outside-out single-channel recordings GluA2(E)/ γ2, to further characterize the inhibition mechanism at the single-channel level. GluA2(E)/ γ2 single channel in the presence of CTZ and a saturating concentration of glutamate (10 mM) predominantly populates the higher conductance levels (Fig. 4C, blue) similar to GluA2(Q) in presence of CTZ (Fig. 1M). In the presence of memantine, the openings were brief and populated lower conductance states (Fig. 4C, pink). Amplitude histograms show that the receptor populates primarily low conductance states in the presence of memantine (Fig. 4D). These

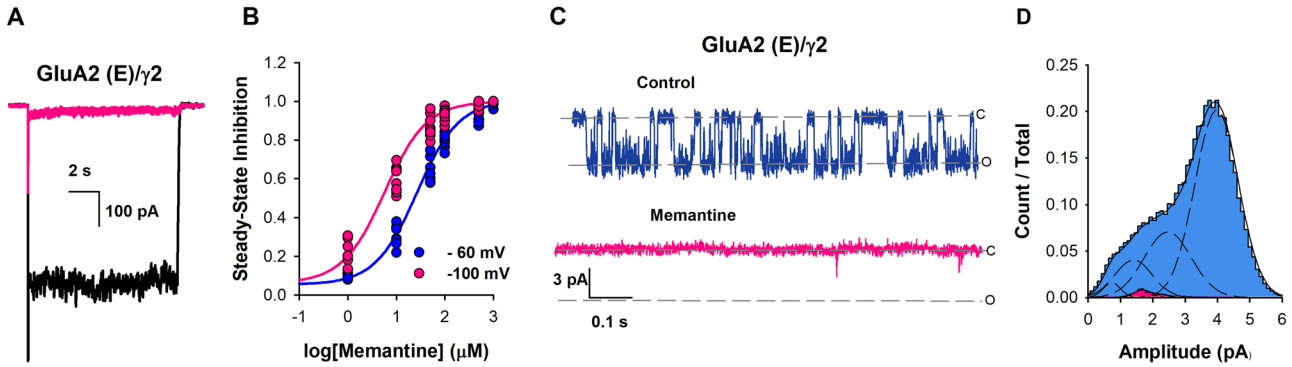

Fig. 4 | Memantine inhibition of GluA2 (E) /γ2. A Representative whole-cell recordings in response to 10 mM glutamate alone (black) or in the presence of 500 μM of memantine (pink). **B** The dose dependence of memantine inhibition on GluA2 (E) /γ2 at −60 (blue) and −100 (pink) mV, with IC_{50} 25 ± 2 μM and 5.7 ± 1 μM, respectively. Each dot represents data from a different cell. **C** Single-channel currents were recorded from GluA2 (E) /γ2 during continuous application of 10 mM glutamate alone (blue) and in the presence 500 μM of memantine (pink). Openings are shown as downward deflections. **D** Amplitude histogram from the single channel recordings showing conductance ($n = 5$).

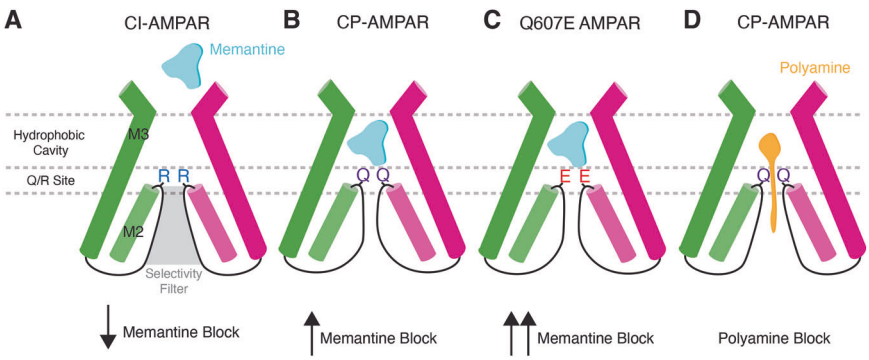

Fig. 5 | Mechanisms of channel block in AMPARs. A Presence of arginine at the Q/R site in CI-AMPARs dramatically reduces the efficacy of memantine block. **B** Glutamine at the Q/R site in CP-AMPARs enables memantine inhibition in CP-AMPARs by directly coordinating memantine in the hydrophobic pocket. Memantine binding also narrows the selectivity filter. **C** The Q607E mutation increases memantine's inhibition efficacy. **D** Polyamines block CP-AMPARs through coordination of the polyamine tail in the selectivity filter and the hydrophobic heads being coordinated in the channel hydrophobic cavity.

measurements support the inhibition by binding to the open channel form of GluA2(E)/ γ2 the receptor similar to that seen for GluA2(Q).

This data not only supports the mechanism of action observed from our cryo-EM data and functional studies, but also points to the possible utility of memantine in attenuating AMPAR gain of function in the Q607E mutant.

Discussion

AMPARs are dynamic complexes capable of shifting between different subunit assemblies consisting of homo- or heteromeric combinations of GluA1 and GluA2 or GluA2 and GluA3 subunits[1,2]. In mature neurons, AMPARs are primarily calcium-impermeable, due to the presence of GluA2 subunits which undergo RNA editing at site 607 (Q/R)[6–11,36,37]. In isolation, CP-AMPARs desensitize more quickly and hence may not contribute significantly to an increase in calcium influx. However, when these receptors are in complex with auxiliary subunits such as γ2 and γ8 they have slower desensitization, higher residual currents, and higher single-channel conductance, leading to increased Ca^{2+} influx. This increase in calcium permeability contributes to neuronal excitability, synaptic plasticity, and neuronal survival. Thus, targeting CP-AMPARs is a critical therapeutic strategy.

Here we show that memantine, an FDA-approved drug classified as an uncompetitive antagonist of NMDARs, also inhibits GluA2 CP-AMPARs albeit at higher concentrations. Through electrophysiology and cryo-EM, we demonstrate that memantine acts as an open channel blocker and shares similarities with the mechanism of NMDAR inhibition, such as its voltage dependence and steric effects[12,13]. However, in contrast to the memantine inhibition in NMDA receptors, inhibition of GluA2 CP-AMPAR currents does not show the biexponential recovery from inhibition as well as pH effect of this recovery, thus suggesting that the second membrane pathway seen in NMDARs is not seen in AMPAR inhibition by memantine.

Through cryo-EM on CP-AMPARs activated in the presence of memantine, we precisely delineate the blocking mechanism. CI-AMPARs have arginine residues at the Q/R site, which dramatically lowers the memantine inhibition (Fig. 5A). CP-AMPARs, which have glutamine at the Q/R site, have significantly increased affinity for memantine, which directly interacts with the Q/R site (Fig. 5B). This causes rearrangement of the Q/R site, and narrows the selectivity filter below. Memantine's hydrophic tricyclodecane cage sits in the hydrophobic cavity of the ion channel, immediately above the Q/R site. This likely prevents the coordination of calcium ions and water around the channel gate[34]. Importantly, a genetic mutation in GluA2 (Q607E) that causes severe neurodevelopmental disorders, occurs directly at the Q/R site. We show that memantine block is significantly increased in Q607E CP-AMPARs, suggesting its potential therapeutic utility in conditions characterized by aberrant AMPA receptor activity in some genetic channel mutations (Fig. 5C).

We also show that other NMDAR blockers such as ketamine or MK801 do not show significant inhibition of CP-AMPARs in the concentration range where they inhibit NMDARs. This adds possible

pathway that may contribute to the differences between the two inhibitors that needs to be further explored.

The cryo-EM data also shows memantine block in CP-AMPARs is unique from polyamine block in CP-AMPARs. Polyamine derivates partially permeate the channel where the polyamines act as cations that are coordinated by the selecitivity filter. A hydrophobic head above the polyamine chain sits in the channel hydrophobic cavity, effectively plugging the channel (Fig. 5D). This is in contrast to memantine, which interacts with the Q/R site directly, narrows the selectivity filter, and blocks the channel.

In conclusion, our study presents an examination of memantine's pharmacological profile of AMPA receptors, revealing its novel role as an inhibitor of CP-AMPARs. While memantine exhibits 10 to 20 percent inhibition at clinically relevant concentrations, these studies provide a foundation for further drug development based on the memantine chemistry.

Methods

Constructs

The rat GluA2 flip (Q) construct was used to generate the GluA2(R), GluA2(E) and GluA2(A622T) constructs using standard site-directed mutagenesis. The tandem constructs for GluA2 with γ2 and γ8 were generated using a Gly-Ser linker between the C-terminus of GluA2 and the N-terminus using Gibson Assembly protocol. The mutations and integrity of the constructs were confirmed by sequencing (Genewiz).

Cell culture

The electrophysiological experiments were performed using HEK 293 T cells (American tissue culture corporation). The procedure for maintenance and transfection of the HEK-293T cells has been previously described[20,38]. Briefly, HEK-293 cells were grown to 40–50% confluency in DMEM (GenDEPOT) supplemented with 10% FBS (GenDEPOT) and penicillin/streptomycin (Invitrogen) and transfected with GluA2(Q), GluA2(A622T), GluA2(Q)/ γ2, GluA2(Q)/ γ8, or GluA2(R), GluA2(E), and GluA1 cotransfected with γ2 or γ8 along with GFP using lipofectamine 2000 (Invitrogen). Cells were re-plated after 4-6 h at a low density in fresh media containing NBQX. For single-channel recordings, cells were grown on poly-D-lysine–coated dishes, while no poly-lysine was used for whole-cell recordings. The electrophysiological experiments were performed 24-48 h after transfection.

Electrophysiology

Whole-cell patch-clamp recordings with HEK-293T cells were obtained from HEK293T cells using 3–5 MΩ resistance borosilicate glass pipettes. Intracellular buffer used for the whole cell recordings contained 135 mM CsF, 33 mM CsCl, 2 mM $MgCl_2$,1 mM $CaCl_2$, 11 mM EGTA, and 10 mM HEPES, pH 7.4, while extracellular buffer contained 150 mM NaCl, 4 mM KCl, 2 mM $CaCl_2$, and 10 mM HEPES, pH 7.4. Solution exchange was achieved using a perfusion Fast-Step system (Warner Instruments) with the cells being lifted and brought near the perfusion system. We determined the time for solution exchange with an open pipette using buffers with different salt solutions (data shown in Fig. S6). All recordings were performed at room temperature with a holding potential of −60 mV, using an Axopatch 200B amplifier (Molecular Devices). The currents were acquired at 10 kHz using pCLAMP10 software (Molecular Devices), and filtered at 5 kHz.

For single-channel recording, the electrophysiological recordings were performed in the outside-out patch-clamp configuration, at a holding potential was −100 mV. Buffers and solution concentrations were the same as those used for whole-cell recordings. Data were acquired at 50 kHz and low-pass filtered at 10 kHz (Axon 200B and Digidata 1550 A; Molecular Devices) and further filtered at 1 kHz during analysis. The recordings were idealized using the segmental k-means algorithm of QuB[39].

Data analysis

Dose-response curves were generated using $E_{inhibition}$ as a function of memantine concentrations. For these $E_{inhibition}$ was determined using the following equation:

$$E_{inhibition} = 1 - \frac{I_{MEM}}{I_{control}} \quad (1)$$

Where I_{MEM} is the steady-state current in the presence of Memantine and $I_{control}$ is the steady-state current in the absence of Memantine.

IC_{50} was determined from the dose-response curves using the Hill equation:

$$E_{inhibition} = \frac{E_{min} + (E_{max} - E_{min})}{(1 + 10^{n(LogIC_{50} - C)})} \quad (2)$$

Where $E_{inhibition}$ is steady-state inhibition as defined by Eq. 1, E_{min} is the lowest value for steady-state inhibition, E_{max} is the maximum value for steady-state inhibition, IC_{50} is the concentration of Memantine at half-maximal inhibition, and C is the concentration of Memantine.

Statistics

At least three recordings were obtained for each condition studied from at least 3 different days. All electrophysiological data were statistically analyzed using the paired t-test. These tests were performed using SigmaPlot10 (v10; Systat Software, Inc, USA). For all tests, a *p*-value of 0.05 was considered significant, and a *p*-value of 0.001 was considered highly significant.

Sources of Drugs. Memantine (Sigma-Aldrich), D-APV (Abcam), glutamate (Sigma-Aldrich), TTX (Tocris), MK-801 (Sigma-Aldrich) and cyclothiazide (CTZ) (Sigma-Aldrich) were commercially available. *N*,*N*,*N*,3,5-pentamethyladamantan-1-ammonium iodide (trimethylmemantine, TMM) was synthesized and purified as previously reported[27].

Protein expression and purification

$GluA2\text{-}\gamma2_{EM}$ bacmid and P1 baculovirus were prepared as previously described[28,30–33]. Protein expression in mammalian Expi293F GNTI$^-$ cells (Gibco, A39240) was induced by the addition of P1 baculovirus in a 1:10 ratio of P1 virus to culture volume. Cells were grown at 37 °C in 5% CO_2. 10 mM sodium butyrate (Sigma, 303410) and 2 μM ZK 20075 (Tocris, 2345) were added to cells 12–24 h post-induction, then transferred to 30 °C in 5% CO_2. Cells were harvested 72 h post-induction by centrifugation (5000 *g*, 20 minutes at 4 °C), and washed with 1X PBS (pH 7.4) with protease inhibitors (0.8 μM aprotinin, 2 μg ml^{-1} leupeptin, 2 μM pepstatin A, and 1 mM phenylmethylsulfonyl fluoride). Pellets were stored at −80 °C until purification. Pellets were thawed at 22 °C, rotating in lysis buffer (150 mM NaCl, 20 mM Tris pH 8.0) with protease inhibitors, described above. Cells were lysed with a blunt probe sonicator (1 s on, 1 s off for 1 minute, 20 W power, total of 3 cycles). Lysed cells were clarified by centrifugation (4800 *g*, 20 minutes at 4 °C). Supernatant was collected and ultracentrifugized to isolate membranes (125,000 *g*, 50 minutes at 4 °C). Membrane fraction was first homogenized (Fisherbrand 150 Handheld Homogenizer) with 150 mM NaCl and 20 mM Tris pH 8.0, and then solubilized with 150 mM NaCl, 20 mM Tris pH 8.0, 1% *n*-dodecyl-ß-D-maltopyranoside (DDM; Anatrace, D310) and 0.2% cholesteryl hemisuccinate Tris salt (CHS; Anatrace, CH210), via constant stirring for 2 h at 4 °C. Sample was ultracentrifugized (125,000 *g*, 50 minutes at 4 °C) to separate solubilized protein. Supernatant was incubated with 1.125 ml of Strep-Tactin XT 4Flow resin (IBA, 2-5010) per 1 L of cells overnight, rotating at 4 °C. The resin was washed with 10 column volumes of 150 mM NaCl, 20 mM Tris pH 8.0, and 0.01% glycol-disgenin (GDN; Anatrace, GDN101) buffer. Sample was eluted with the same buffer, supplemented with 50 mM biotin. Eluate was concentrated to 500 μl volume. eGFP and

Strep Tag II were then cleaved by addition of thrombin (1:200 w/w), and incubated at 22 °C for 1 h. The sample was then loaded onto a size-exclusion chromatography column (Superose 6 Increase 10/300; Cytiva, 29091596) that was equilibrated with 150 mM NaCl, 20 mM Tris pH 8.0, and 0.01% glycol-disgenin (GDN) buffer. Peak fractions were pooled and concentrated to 4 mg ml^{-1}.

Cryo-EM sample preparation and data collection

UltrAuFoil 200 mesh R 2/2 grids (Electron Microscopy Services, Q250AR2A) were plasma treated in a Pelco Easiglow (25 mA, 120 s glow time and 20 s hold time; Ted Pella, 91000). Purified sample at 4 mg ml^{-1} was supplemented with 100 μM CTZ and 500 μM memantine before ultracentrifugation (75,000 *g*, 45 minutes at 4 °C). Immediately prior to plunge-freezing, the sample was spiked with 1 mM Glu (pH 7.4). 3 μL of reaction mixture was applied to each grid. Grids were prepared using an FEI Vitrobot Mark IV (Thermo Fisher Scientific; wait time, 25 s; blot force, 8; blot time, 4 s) at 8 °C and 100% humidity.

Grids were imaged with a 300-kV Titan Krios 3i microscope equipped with a Falcon 4i camera and a Selectric energy filter set to 10-eV slit width. Micrographs were collected with a dose rate of 8.64 e^-/pixel/s and a total dose of 40.00 e^-/Å^2. We collected a total of 7009 micrographs (0.93 Å/pixel). Automated collection was performed with EPU software from Thermo Fisher Scientific.

Cryo-EM image processing & model building

Cryosparc was used for all aspects of cryo-EM image processing. Refer to figure S4 and Table S1 for details. All aspects of modeling, refinement, and analysis were performed with ChimeraX, Isolde, Coot, and Phenix made accessible through the SBgrid consortium[40–45]. See Table S1 for details. The GluA2-γ2$_{EM}$ activated state (pdb 5WEO) was used as a starting model. Model quality was assessed with MolProbity[46]. Pore measurements were made with HOLE[47].

Reporting summary

Further information on research design is available in the Nature Portfolio Reporting Summary linked to this article.

Data availability

All electrophysiology data are included in main manuscript or in supplementary data. All cryo-EM reconstructions are deposited into the Electron Microscopy Data Bank EMD-47520 and EMD-47521. The atomic coordinates have been deposited in the Protein Data Bank (PDB) under the accession codes 9E4Y and 9E4Z. Source Data are provided with this paper.

References

1. Hansen, K. B. et al. Structure, function, and pharmacology of glutamate receptor ion channels. *Pharm. Rev.* **73**, 298–487 (2021).
2. Twomey, E. C., Yelshanskaya, M. V. & Sobolevsky, A. I. Structural and functional insights into transmembrane AMPA receptor regulatory protein complexes. *J. Gen. Physiol.* **151**, 1347–1356 (2019).
3. Iacobucci, G. J. & Popescu, G. K. NMDA receptors: linking physiological output to biophysical operation. *Nat. Rev. Neurosci.* **18**, 236–249 (2017).
4. Burnashev, N., Monyer, H., Seeburg, P. H. & Sakmann, B. Divalent ion permeability of AMPA receptor channels is dominated by the edited form of a single subunit. *Neuron* **8**, 189–198 (1992).
5. Cull-Candy, S. G. & Farrant, M. Ca2+-permeable AMPA receptors and their auxiliary subunits in synaptic plasticity and disease. *J. Physiol.* **599**, 2655–2671 (2021).
6. Gaisler-Salomon, I. et al. Hippocampus-specific deficiency in RNA editing of GluA2 in Alzheimer's disease. *Neurobiol. Aging* **35**, 1785–1791 (2014).
7. Yamashita, T. & Kwak, S. Cell death cascade and molecular therapy in ADAR2-deficient motor neurons of ALS. *Neurosci. Res.* **144**, 4–13 (2019).
8. Konen, L. M. et al. A new mouse line with reduced GluA2 Q/R site RNA editing exhibits loss of dendritic spines, hippocampal CA1-neuron loss, learning and memory impairments and NMDA receptor-independent seizure vulnerability. *Mol. Brain* **13**, 27 (2020).
9. Maas, S., Patt, S., Schrey, M. & Rich, A. Underediting of glutamate receptor GluR-B mRNA in malignant gliomas. *Proc. Natl Acad. Sci. USA* **98**, 14687–14692 (2001).
10. Li, L. et al. α2δ-1 switches the phenotype of synaptic AMPA receptors by physically disrupting heteromeric subunit assembly. *Cell Rep.* **36**, 109396 (2021).
11. Selvaraj, B. T. et al. C9ORF72 repeat expansion causes vulnerability of motor neurons to Ca(2+)-permeable AMPA receptor-mediated excitotoxicity. *Nat. Commun.* **9**, 347 (2018).
12. Bormann, J. Memantine is a potent blocker of N-methyl-D-aspartate (NMDA) receptor channels. *Eur. J. Pharm.* **166**, 591–592 (1989).
13. Parsons, C. G., Gruner, R., Rozental, J., Millar, J. & Lodge, D. Patch clamp studies on the kinetics and selectivity of N-methyl-D-aspartate receptor antagonism by memantine (1-amino-3,5-dimethyladamantan). *Neuropharmacology* **32**, 1337–1350 (1993).
14. Aracava, Y., Pereira, E. F., Maelicke, A. & Albuquerque, E. X. Memantine blocks alpha7* nicotinic acetylcholine receptors more potently than n-methyl-D-aspartate receptors in rat hippocampal neurons. *J. Pharm. Exp. Ther.* **312**, 1195–1205 (2005).
15. Reiser, G., Binmöller, F.-J. & Koch, R. Memantine (1-amino-3,5-dimethyladamantane) blocks the serotonin-induced depolarization response in a neuronal cell line. *Brain Res.* **443**, 338–344 (1988).
16. Ferrer-Montiel, A. V., Merino, J. M., Planells-Cases, R., Sun, W. & Montal, M. Structural determinants of the blocker binding site in glutamate and NMDA receptor channels. *Neuropharmacology* **37**, 139–147 (1998).
17. Chen, L. et al. Stargazin regulates synaptic targeting of AMPA receptors by two distinct mechanisms. *Nature* **408**, 936–943 (2000).
18. Jackson, A. C. & Nicoll, R. A. The expanding social network of ionotropic glutamate receptors: TARPs and other transmembrane auxiliary subunits. *Neuron* **70**, 178–199 (2011).
19. Herguedas, B. et al. Mechanisms underlying TARP modulation of the GluA1/2-γ8 AMPA receptor. *Nat. Commun.* **13**, 734 (2022).
20. Carrillo, E. et al. Mechanism of modulation of AMPA receptors by TARP-gamma8. *J. Gen. Physiol.* **152**, e201912451 (2020).
21. Coombs, I. D., MacLean, D. M., Jayaraman, V., Farrant, M. & Cull-Candy, S. G. Dual Effects of TARP gamma-2 on glutamate efficacy can account for AMPA receptor autoinactivation. *Cell Rep.* **20**, 1123–1135 (2017).
22. MacLean, D. M., Ramaswamy, S. S., Du, M., Howe, J. R. & Jayaraman, V. Stargazin promotes closure of the AMPA receptor ligand-binding domain. *J. Gen. Physiol.* **144**, 503–512 (2014).
23. Shaikh, S. A. et al. Stargazin modulation of AMPA receptors. *Cell Rep.* **17**, 328–335 (2016).
24. Zhang, D. et al. Modulatory mechanisms of TARP γ8-selective AMPA receptor therapeutics. *Nat. Commun.* **14**, 1659 (2023).
25. Salpietro, V. et al. AMPA receptor GluA2 subunit defects are a cause of neurodevelopmental disorders. *Nat. Commun.* **10**, 3094 (2019).
26. Hu, W. & Bean, B. P. Differential control of axonal and somatic resting potential by voltage-dependent conductances in cortical layer 5 pyramidal neurons. *Neuron* **97**, 1315–1326 (2018).
27. Wilcox, M. R. et al. Inhibition of NMDA receptors through a membrane-to-channel path. *Nat. Commun.* **13**, 4114 (2022).
28. Hale, W.D. et al. Allosteric competition and inhibition in AMPA receptors. *Nat. Struct. Mol. Biol.* **31**, 1669–1679 (2024).

29. Yelshanskaya, M. V., Patel, D. S., Kottke, C. M., Kurnikova, M. G. & Sobolevsky, A. I. Opening of glutamate receptor channel to subconductance levels. *Nature* **605**, 172–178 (2022).
30. Twomey, E. C., Yelshanskaya, M. V., Vassilevski, A. A. & Sobolevsky, A. I. Mechanisms of channel block in calcium-permeable AMPA receptors. *Neuron* **99**, 956–968.e4 (2018).
31. Twomey, E. C., Yelshanskaya, M. V., Grassucci, R. A., Frank, J. & Sobolevsky, A. I. Structural bases of desensitization in AMPA receptor-auxiliary subunit complexes. *Neuron* **94**, 569–580.e5 (2017).
32. Twomey, E. C., Yelshanskaya, M. V., Grassucci, R. A., Frank, J. & Sobolevsky, A. I. Channel opening and gating mechanism in AMPA-subtype glutamate receptors. *Nature* **549**, 60–65 (2017).
33. Twomey, E. C., Yelshanskaya, M. V., Grassucci, R. A., Frank, J. & Sobolevsky, A. I. Elucidation of AMPA receptor-stargazin complexes by cryo-electron microscopy. *Science* **353**, 83–86 (2016).
34. Nakagawa, T., Wang, X. T., Miguez-Cabello, F. J. & Bowie, D. The open gate of the AMPA receptor forms a Ca(2+) binding site critical in regulating ion transport. *Nat. Struct. Mol. Biol.* **31**, 688–700 (2024).
35. Chou, T. H. et al. Structural insights into binding of therapeutic channel blockers in NMDA receptors. *Nat. Struct. Mol. Biol.* **29**, 507–518 (2022).
36. Ceprian, M. & Fulton, D. Glial cell AMPA receptors in nervous system health, injury and disease. *Int J. Mol. Sci.* **20**, 2450 (2019).
37. Ghirardini, E. et al. Mutant prion proteins increase calcium permeability of AMPA receptors, exacerbating excitotoxicity. *PLoS Pathog.* **16**, e1008654 (2020).
38. Carrillo, E., Bhatia, N. K., Akimzhanov, A. M. & Jayaraman, V. Activity dependent inhibition of AMPA receptors by Zn(2). *J. Neurosci.* **40**, 8629–8636 (2020).
39. Qin, F. Restoration of single-channel currents using the segmental k-means method based on hidden Markov modeling. *Biophys. J.* **86**, 1488–1501 (2004).
40. Pettersen, E. F. et al. UCSF ChimeraX: structure visualization for researchers, educators, and developers. *Protein Sci.* **30**, 70–82 (2021).
41. Croll, T. I. ISOLDE: a physically realistic environment for model building into low-resolution electron-density maps. *Acta Crystallogr D. Struct. Biol.* **74**, 519–530 (2018).
42. Emsley, P. & Cowtan, K. Coot: model-building tools for molecular graphics. *Acta Crystallogr D. Biol. Crystallogr* **60**, 2126–2132 (2004).
43. Liebschner, D. et al. Macromolecular structure determination using X-rays, neutrons and electrons: recent developments in Phenix. *Acta Crystallogr D. Struct. Biol.* **75**, 861–877 (2019).
44. Afonine, P. V. et al. Real-space refinement in PHENIX for cryo-EM and crystallography. *Acta Crystallogr D. Struct. Biol.* **74**, 531–544 (2018).
45. Morin, A. et al. Collaboration gets the most out of software. *Elife* **2**, e01456 (2013).
46. Williams, C. J. et al. MolProbity: more and better reference data for improved all-atom structure validation. *Protein Sci.* **27**, 293–315 (2018).
47. Smart, O. S., Neduvelil, J. G., Wang, X., Wallace, B. A. & Sansom, M. S. HOLE: a program for the analysis of the pore dimensions of ion channel structural models. *J. Mol. Graph* **14**, 376 (1996).

Acknowledgements

This study was supported by National Institute of Health (NIH) Grants R35 GM122528 to V.J, NIH F99NS130928 to C.U.G. E.C.T is supported by the NIH (grant # R35GM154904), the Searle Scholars Program (Kinship Foundation #22098168), and the Diana Helis Henry Medical Research Foundation (#142548). Cryo-EM data was collected at the Beckman Center for Cryo-EM at Johns Hopkins.

Author contributions

E.C. (memantine electrophysiology study design, electrophysiological recordings, data analysis, and writing), A.M.R. (cryo-EM study design, protein purification, cryo-EM, data analysis), C.U.G. (cloning and cell culture), A.L.T. (design and synthesis of Trimethylmemantine), S.V. (design of Trimethylmemantine and writing), E.C.T. (cryo-EM study design, data analysis, writing), V.J. (memantine electrophysiology study design and writing).

Competing interests

The authors declare no competing interests.

Additional information

Supplementary information The online version contains supplementary material available at https://doi.org/10.1038/s41467-025-60543-5.

Correspondence and requests for materials should be addressed to Elisa Carrillo, Edward C. Twomey or Vasanthi Jayaraman.

Peer review information *Nature Communications* thanks the anonymous reviewer(s) for their contribution to the peer review of this work. A peer review file is available.